Neural basis of global resting-state fMRI activity

Marieke L. Schölvinck[a,b], Alexander Maier[a], Frank Q. Ye[c], Jeff H. Duyn[d], and David A. Leopold[a,c,1]

[a]Unit on Cognitive Neurophysiology and Imaging, Laboratory of Neuropsychology, National Institute of Mental Health, National Institutes of Health, Bethesda, MD 20892; [b]Institute of Ophthalmology, University College London, London EC1V 9EL, United Kingdom; [c]Neurophysiology Imaging Facility, National Institute of Mental Health, National Institute of Neurological Disorders and Stroke, and National Eye Institute, National Institutes of Health, Bethesda, MD 20892; and [d]Section on Advanced Imaging, Laboratory of Functional and Molecular Imaging, National Institute of Neurological Disorders and Stroke, National Institutes of Health, Bethesda, MD 20892

Edited by Robert G. Shulman, Yale University School of Medicine, New Haven, CT, and approved April 13, 2010 (received for review November 12, 2009)

Functional MRI (fMRI) has uncovered widespread hemodynamic fluctuations in the brain during rest. Recent electroencephalographic work in humans and microelectrode recordings in anesthetized monkeys have shown this activity to be correlated with slow changes in neural activity. Here we report that the spontaneous fluctuations in the local field potential (LFP) measured from a single cortical site in monkeys at rest exhibit widespread, positive correlations with fMRI signals over nearly the entire cerebral cortex. This correlation was especially consistent in a band of upper gamma-range frequencies (40–80 Hz), for which the hemodynamic signal lagged the neural signal by 6–8 s. A strong, positive correlation was also observed in a band of lower frequencies (2–15 Hz), albeit with a lag closer to zero. The global pattern of correlation with spontaneous fMRI fluctuations was similar whether the LFP signal was measured in occipital, parietal, or frontal electrodes. This coupling was, however, dependent on the monkey's behavioral state, being stronger and anticipatory when the animals' eyes were closed. These results indicate that the often discarded global component of fMRI fluctuations measured during the resting state is tightly coupled with underlying neural activity.

cortex | electrophysiology | local field potential | functional connectivity | monkey

The mammalian cerebral cortex is subdivided into specialized regions for various cognitive functions, such as the processing of sensory stimuli, memory, and the execution of movements. This functional specialization notwithstanding, the brain does not cease to show pronounced dynamic activity in the absence of cognitive or sensory stimulation. Significant ongoing spontaneous activity has been demonstrated using optical (1, 2), electrophysiological (3–5), and functional imaging (6, 7) techniques in several species under a variety of behavioral states. FMRI allows for visualization of large-scale, spatial patterns of such intrinsic activity, which is achieved by mapping patterns of activity covariation between brain regions. The temporal correlation between fluctuations in different regions is then often taken as a measure of "functional connectivity" between the corresponding brain areas (8–11). These fluctuations typically exhibit their highest intervoxel coherence at low temporal frequencies (<0.1 Hz) and can be observed during alertness (12, 13), sleep (14, 15), light sedation (16), and general anesthesia (17, 18). Experiments are beginning to address the spatiotemporal characteristics of these spontaneous fluctuations in animal models (19–21), with initial studies in macaques suggesting a human-like pattern of functional connectivity (7, 22).

In humans, spontaneous activity is typically investigated in the so-called resting state, a term that is only loosely defined and which typically amounts to a subject lying in the scanner without an explicit stimulus or task. Under these conditions, analysis of spatiotemporal coherence of fMRI activity reveals several distinct domains of correlated activity in the brain, sometimes described as networks (23–25). These include a so-called default-mode network (10), attentional networks (12), networks in visual (26, 27), auditory (28), and somatomotor (6, 29) cortex, and networks including the thalamus (30), cerebellum (31), and basal ganglia (32). Although fMRI activity covariation can be attributed to many factors, it is generally ascribed to neural activity stemming from known anatomical connections (33, 34) and, as such, appears to be fundamental to the brain's functional organization.

In the course of investigating functional networks, it is customary to first remove the contribution of so-called global signal fluctuations. These slow undulations affect large swathes of the brain and stem in part from nonneural sources such as instability in the MR measurement and instability in heart rate and respiration (35–37). The mathematical removal of these global signal fluctuations can sharpen stimulus responses and increase the visibility of functional networks (38); however, such data processing must be applied with caution, as global signal regression can profoundly affect the spatial pattern, and even polarity, of the measured correlations (39, 40). In addition to the contribution of nonneural sources, some aspects of spontaneous fMRI fluctuations appear to arise from underlying neural activity (4, 35, 41–43). In particular, electrophysiological studies in both humans and animals point to slow fluctuations in high-frequency "gamma" local field potential (LFP) power (>30 Hz) as exhibiting spatial coherence over long timescales (4, 42, 43), with some evidence suggesting that this coherence is strongest between functionally related areas (42). Recently, a strong link between spontaneous fMRI fluctuations and neural activity, including both gamma-range LFP and spiking, was demonstrated directly in a study simultaneously measuring electrophysiological and fMRI signals in the anesthetized monkey (41).

Here we show, using combined LFP/fMRI measurements in awake monkeys at rest, that spontaneous neural and fMRI signals are not only correlated but that the neural signal from a single cortical site is coupled to global fMRI fluctuations over large swathes of the cerebral cortex. We found such global coupling with electrodes in the occipital, parietal, and frontal lobes, with consistent correlation found only for certain LFP frequencies, in particular those in the upper gamma frequency range (40–80 Hz). These findings demonstrate that global signal fluctuations commonly observed in human resting-state fMRI data can be directly linked to neural activity fluctuations in the cerebral cortex.

Results

Three female rhesus macaque monkeys (A, V, and S) were tested in a 4.7 T vertical scanner (Bruker BioSpec 47/60) using standard echoplanar imaging (EPI) fMRI sequences. Each monkey was implanted with one to three arrays of MR-compatible multicontact electrodes (NeuroNexus Technologies), allowing for the measurement of neural signals during the fMRI sessions (*Methods*). The animals were trained to sit quietly in the scanner, having been

Author contributions: M.L.S., A.M., J.H.D., and D.A.L. designed research; M.L.S., F.Q.Y., and D.A.L. performed research; F.Q.Y. contributed new reagents/analytic tools; M.L.S., J.H.D., and D.A.L. analyzed data; and M.L.S., A.M., and D.A.L. wrote the paper.

The authors declare no conflict of interest.

This article is a PNAS Direct Submission.

[1]To whom correspondence should be addressed. E-mail: leopoldd@mail.nih.gov.

This article contains supporting information online at www.pnas.org/lookup/suppl/doi:10.1073/pnas.0913110107/-/DCSupplemental.

previously acclimated to the scanner environment, and had no particular behavioral requirements. Together, the animals participated in a total of 67 combined electrophysiology/fMRI runs, with each run lasting 30 min, over a period of roughly 1 year. We were primarily interested in the spatiotemporal covariation between ongoing neural signals measured with the implanted electrodes and the ongoing hemodynamic signals measured with fMRI.

Correlation as a Function of LFP Frequency Range. A previous study (41) showed strong correlation between the fMRI signal measured in V1 and LFP power in the high gamma (40–80 Hz) frequency range. To examine fMRI correlation with other bands of the LFP spectrum, we estimated LFP power uniformly across frequencies between 2 and 100 Hz by computing the fast Fourier transform (FFT) of the LFP signal (see *SI Text*). Comparing the slow temporal variation in power of each of these frequencies with that of the fMRI signal from a region of interest (ROI) a few millimeters away from the V1 electrode (Fig. 1*A*) revealed the LFP frequency dependence of this correlation (Fig. 2*A*). Specifically, the data demonstrated three broad frequency domains in which the LFP differed markedly in its relationship to the fMRI signal: (*i*) a low-frequency band (2–15 Hz) showing a strong positive correlation to the fMRI signal, (*ii*) a middle-range-frequency band (15–40 Hz) with a variable and slightly negative correlation, and (*iii*) a high-frequency band (gamma, 40–80 Hz) that showed a consistent positive correlation. These differences in correlation levels could not be attributed to signal-to-noise differences based on the frequency distribution of LFP power, because its 1/f distribution (Fig. S1) would predict lower signal-to-noise in the gamma range than in the middle range. Cross-correlation functions from the band-limited power (BLP) (*Methods*) computed over the three bands are shown in Fig. 2*B*, with data shown separately for each monkey. In the high-frequency band, there was a consistent correlation between the V1 LFP and fMRI signals, with a mean peak correlation of between 0.2 and 0.3 for each of the three animals. The time course qualitatively resembled the hemodynamic impulse-response function (44, 45), peaking when the fMRI signal lagged the neural signal by ≈7–8 s, indicating that events in the fMRI signal followed those in the neural signal. Based on the length of the time series, the threshold of spurious correlations was 0.07 (*t* test, $P < 0.05$). Responses from the other frequency bands also showed significant correlations to the fMRI signal; however, in contrast to the high-frequency band, the strength and polarity of their correlation differed between the three animals. In what follows, we focus on the high-frequency gamma LFP and its correlation with the fMRI signal; data from other frequencies are presented in *SI Text*.

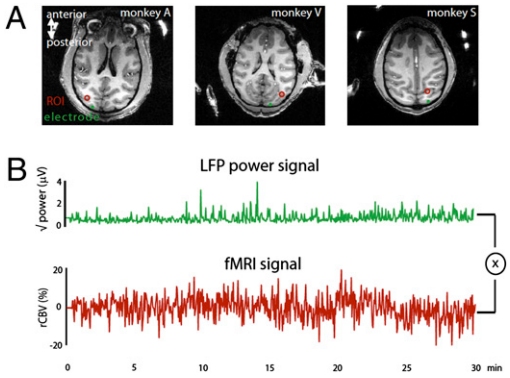

Fig. 1. Simultaneous fMRI and electrophysiology, and data analysis. (*A*) Position of implanted MR-compatible electrodes in V1 and regions of interest for each monkey. (*B*) Example of electrophysiological signal (BLP) and fMRI signal (rCBV) measured in this study. Each signal, collected over the course of 30 min, consisted of 700 data points.

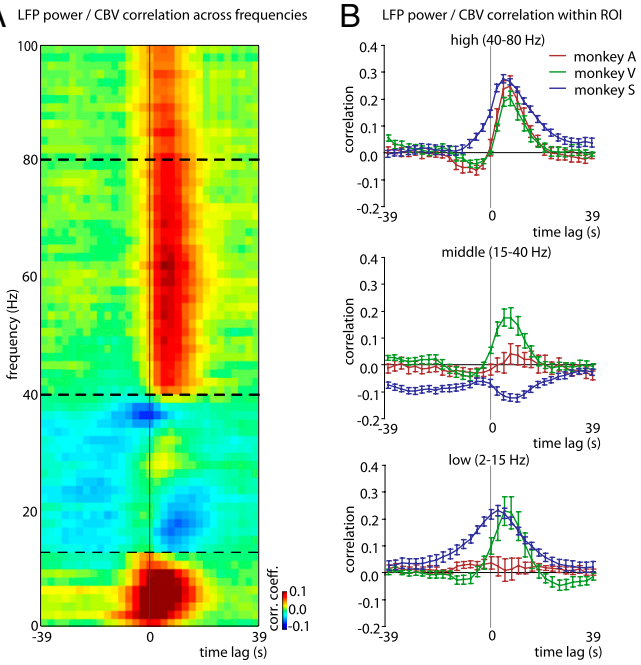

Fig. 2. Cross-correlation between the fMRI (ROI data) and LFP power time courses as a function of LFP constituent frequency. (*A*) Cross-correlation over all frequencies, expressed as a function of temporal lag (abscissa), averaged over all sessions in three monkeys. Dashed horizontal lines indicate apparent divisions between processes corresponding to frequency ranges. These were classified for further analysis as low (2–15 Hz), middle (15–40 Hz), and high (40–80 Hz). (*B*) Cross-correlations, for each of the three monkeys, from band-limited power signals derived from each of the three frequency ranges indicated in *A*.

Widespread fMRI Correlation with Gamma-Range Power. The analysis described above revealed a consistent relationship between the high-frequency LFP and the fMRI signal from the ROI selected a few millimeters away from the electrode. To examine the spatial distribution of this relationship, we separately computed the cross-correlation of the gamma power (40–80 Hz) with each voxel inside and outside the brain, and displayed the results as unthresholded spatial correlation maps over the entire field of view. The result for one session in monkey A is shown in Fig. 3, which reveals a strong correlation not only near the electrode but extending over much of the cortex of both hemispheres (see Figs. S2 and S3 for similar results in monkeys V and S). To assess the significance of these maps, we adjusted the probability of spurious correlations using the Bonferroni method, providing a conservative threshold for spurious correlations of 0.18 (*t* test, $P < 0.05$, corrected). The temporal evolution of this spatial pattern, corresponding to different lags in the cross-correlation function, is shown in Fig. 3*B*. In that figure, the data for the cerebral cortex are plotted on the surface of a 3D reconstruction of the brain for this monkey (see Figs. S2*B* and S3*B* for monkeys V and S). The correlation of the fMRI signal with the low-frequency LFP power (2–15 Hz) showed a similar widespread spatial distribution (Fig. S4), suggesting that this widespread covariation is not restricted to the gamma frequency range. Strong correlation was restricted to the cortex. It was not consistently evident in subcortical structures such as the thalamus, and was much lower for a region of interest in the white matter (Fig. S5).

Similar widespread correlations between LFP power and fMRI activity were observed when the neural signal was obtained from

NEUROSCIENCE

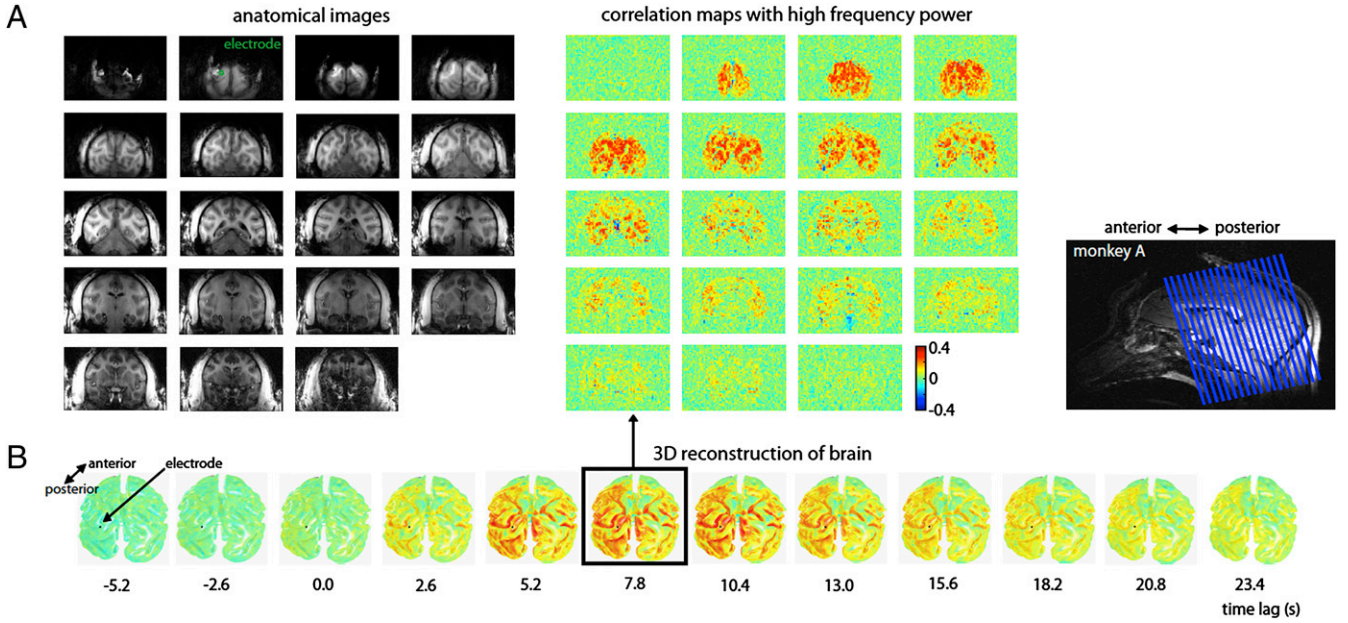

Fig. 3. Spatial extent of the correlation between the neural signal in V1 and spontaneous fMRI fluctuations. (*A*) Correlation maps from one run, obtained at a temporal lag of 7.8 s, are shown for 19 coronal slices in monkey A. The image at the top left corner is from the most posterior slice. The position of the electrode is shown in green on slice 2. Correlation maps from monkeys V and S are shown in Figs. S2 and S3. (*B*) Correlation maps from the same run as a function of temporal lag are shown on an inflated 3D reconstruction of the monkey's brain. The position of the electrode is shown as a black dot. The temporal coupling between the two signals, as well as the large spatial extent of the correlations, are clearly visible.

cortical areas other than V1. Fig. 4*A* shows the mean correlation between gamma-range LFP and fMRI over the entire brain for three electrodes implanted far away from area V1. The LFP signals from the parietal cortex, frontal cortex, and area V4 bore a similar spatial pattern of correlations to the cortical fMRI signal fluctuations as those measured in V1 (the absence of correlation in the occipital lobe of monkey S is due to a magnetic susceptibility artifact in the raw images stemming from the implants). Furthermore, the frequency dependence of this correlation was also similar (i.e., Fig. 4*B* vs. Fig. 2*B*). Interestingly, the LFP/fMRI correlation in occipital lobe voxels was just as strong with the frontal and parietal electrodes as with the occipital electrodes (see frontal electrode correlation map in Fig. S6). This finding highlights the global nature of the LFP/fMRI correlation. Note that the measured posterior-to-anterior gradient reflects the intensity gradient of our radio-frequency (RF) coil, which was optimized for the occipital lobe (Fig. S7). As a result, it is likely that the actual homogeneity of the global correlation is considerably higher than is apparent in Figs. 3 and 4.

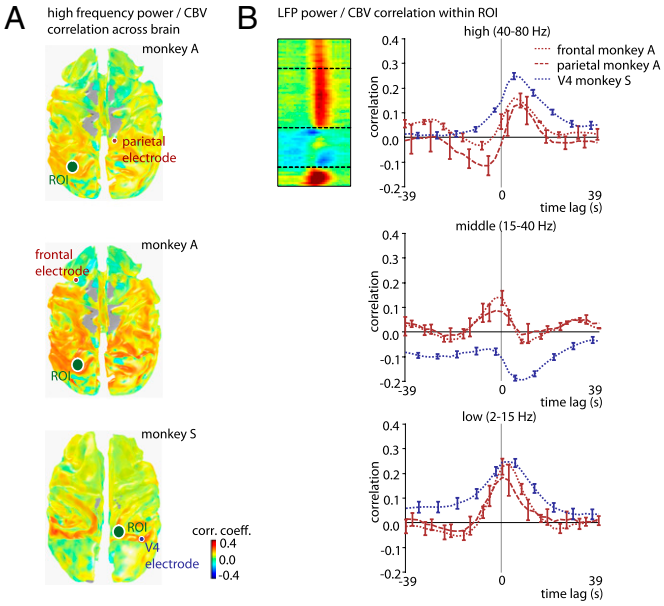

Fig. 4. Spatial extent of the fMRI correlation with high-frequency LFP in frontal area 6d, parietal area 7a, and occipital area V4. (*A*) In all cases, spatial correlations are bilateral and spread over large swathes of the cerebral cortex. (*B*) Cross-correlation functions for three electrodes outside V1, for the three frequency ranges. For details, see Fig. 2. Also, see Figs. S8 and S9 for examples of LFP/fMRI correlations with other electrode contacts in each array.

State Dependence of LFP/fMRI Coupling. Finally, we examined the time course of the high-gamma correlation with fMRI activity in V1, and related it to the animals' state of alertness, which was gauged by the scoring of an infrared video camera feed monitoring the monkey's face throughout the experiment. For the two animals that consistently showed periods of eye opening and closure during the experiments (monkeys A and S), we compared the strength of LFP/fMRI correlations for these periods within a session and between sessions, taking eye opening and closure to indicate the level of alertness. This analysis revealed that the strength of the correlation between the fMRI signal and high-frequency LFP was not constant, but instead changed markedly over time.

Fig. 5*A* shows a running correlation between the two signals for one session in monkey A, computed between the electrode in area V1 and the mean fMRI signal in the ROI (see inset). This analysis revealed that the strength of the correlation varied substantially over a period of several minutes. These changes could not be ascribed to changes in the overall power of the regional cerebral blood volume (rCBV) or LFP signals, which remained similar throughout (Fig. 5*B*, top and middle). However, the change in correlation strength did correspond to the monkey's state of alertness. Specifically, the correlation strength was highest when

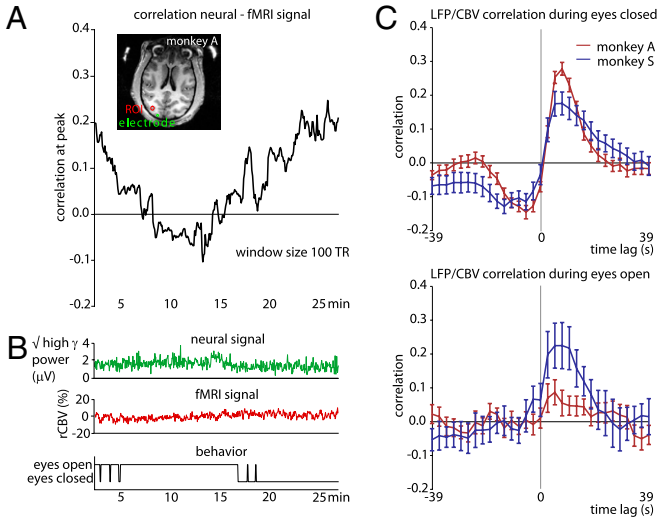

Fig. 5. Nonstationarity of coupling between fMRI and LFP signal. (*A*) Example where the use of a sliding window (100 TR) revealed large changes in the fMRI/LFP correlation strength over the course of a run. (*B*) The corresponding high-frequency LFP power and mean voxel time course from the ROI did not visibly change during this run (top and middle), although the opening and closure of the monkey's eyes appeared linked to the correlation strength (bottom). (*C*) Analysis of all runs from both monkeys A and S revealed stronger neurovascular coupling when the monkeys' eyes were mostly (>80% of the time) closed (top) to when they were mostly open (bottom). Monkey V was excluded from this analysis, as her eyes were never closed for more than a few seconds.

the eyes were closed, and fell to near zero when the eyes were open (Fig. 5*B*, bottom). This change in amplitude was highly consistent across sessions in monkey A (although not in monkey S), whose mean correlation peak was 0.3 during periods of closed eyes but fell to less than 0.1 when the eyes were open in the same sessions (Fig. 5*C*). Aside from the amplitude, another feature of the cross-correlation function depended on the animals' alertness. Namely, during periods of eye closure, there was a significant negative correlation at *negative* time lags, giving the function a distinctly biphasic shape in both monkeys. The significant correlation at negative lags suggests that some aspect of the vascular response consistently *preceded*, and therefore could not be caused by, the corresponding neural events. The basis of this finding is not understood, and it is possible that it reflects higher-level temporal coordination of the LFP and fMRI signals when the eyes are closed, perhaps involving the parallel control of blood flow and cortical activation level.

Discussion

The present results demonstrate a widespread correlation of the gray matter fMRI signal to LFP power sampled from a single position in the cerebral cortex. This effect was seen when the cortical microelectrode was located in the primary visual cortex or elsewhere. The correlation of the low- and high-frequency ranges of the LFP to the rCBV signal was positive, whereas that of the middle range was variable. The tight link between the spontaneous hemodynamic signals and the high-frequency LFP is consistent with previous studies (41, 46). In addition, the low and high LFP frequency bands showing positive correlation with the spontaneous fMRI signal in the present study are similar to those previously observed to carry mutually exclusive information about a complex visual stimulus in the primary visual cortex, suggesting that they reflect distinct types of neural events (47). For the high-frequency range, but not the low one, the lag of 7–8 s of the fMRI signal behind the high-frequency LFP is suggestive of a causal relationship, where a given neural event leads to a corresponding hemodynamic response. It will be of great interest to understand the apparently non- or inversely causal relationship between the two signals in the case of the (*i*) low (2–15 Hz) LFP frequencies and (*ii*) high (40–80 Hz) frequencies during periods of eye closure.

Global Signal Removal. Resting-state fMRI studies routinely remove the spontaneous blood oxygenation level-dependent (BOLD) fluctuations common to large regions of the brain to focus on covariation within so-called functional networks (12, 48). The assumption underlying this data-processing step is that global fMRI fluctuations are caused by nonneural factors, which have been shown to contribute to a portion of the variance (40). However, our data demonstrate that a significant portion of the global signal time course is directly linked to neural activity. This finding has implications for the interpretation of functional networks, and especially for negative (anti-) correlations observed between different functional networks following global signal removal (39, 40). Although it may still be appropriate to remove the shared component in some cases to focus on *differences* in correlation strength, the present findings show that a portion of the global time course is linked to neural activity, and the results of such analyses must therefore be interpreted with caution.

In our measurements, we found that the mean cross-correlation between the LFP and the fMRI signal peaked at about 0.3 in the gray matter, implying that about 10% of the variance in the fMRI signal could be explained by fluctuations in neural activity (corresponding to the square of the correlation coefficient at that time lag). To interpret this correlation magnitude, and to consider what might account for the remainder of the variance, it is important to keep in mind that the LFP and rCBV are fundamentally different types of signals that bear a complex relationship to one another, and that multiple factors serve to lower the measured correlation values. Even under optimal conditions, where the fMRI and neural signals are driven by a strong visual stimulus in a block design, the mean coefficient of determination between them (i.e., fraction of explained variance) was just above 50% (49). During spontaneous activity, multiple factors serve to further decrease the signal correlation. First, any causal connection between the extracellular potential and the fractional blood volume is at best indirect, mediated through any of a number of neurovascular coupling mechanisms whose transduction may be inexact and nonlinear (50). Second, our neural analysis was unlikely to perfectly isolate those processes that drive changes in the rCBV; it is likely that dissecting the LFP into frequency bands is but a crude means of isolating particular types of stochastic (rather than periodic) neural events. Third, other physiological factors, such as changes in blood pressure and heart rate, are also known to contribute to the overall variance of the rCBV signal but are not correlated with the LFP signal (35). Finally, the sluggish hemodynamic responses to neural events are necessarily smoothed and diluted over time. Each of these factors would have the effect of causing a mismatch between measured rCBV and LFP power signals and thereby diminishing the measured peak correlation value. These issues notwithstanding, the shape and approximate magnitude of the cross-correlation was consistent between monkeys and across areas, and was also specific to the gray matter of the cerebral cortex.

Implications for Neurovascular Coupling. Our observation of nonstationarity in the correspondence between the fMRI signal and the underlying neural activity (Fig. 5*C*) has implications for the understanding of neurovascular coupling. The neurophysiological basis of the fMRI signal has been studied almost exclusively in the context of the response to a stimulus, and has revealed that fMRI responses are tightly linked to neural activity, and particularly synaptic activity thought to be reflected in the LFP (44, 46, 51). At the same time, there is growing consensus that the re-

lationship between the fMRI signal and the underlying neural activity is a complex one, because numerous physiological factors contribute to the modulation of microvasculature (50). Indeed, a recent study in monkeys found that vascular responses in the primary visual cortex could be observed in the absence of significant local neural correlates (52). Our findings demonstrate that neurovascular coupling is itself dynamic and subject to behavioral state (see also ref. 53). This adds to recent work showing that correlation patterns in both fMRI (22, 26) and neural (42, 54) signals vary as a function of behavioral state.

Possible Origin and Significance of Resting-State Fluctuations. A possible implication of the coupling between local LFP and global fMRI fluctuations is that the LFP signals are themselves also correlated at a global level. Indeed, widespread coherence in the fluctuations in high-frequency LFP power between cortical sites has been reported previously (4, 43), with indications that these coherent fluctuations show some functional specificity (42). It is natural then to ask: What drives these slow neural fluctuations in the cortex, and what is their purpose? One possibility is that the entire cortex receives neurochemical input from subcortical nuclei, such as the ascending reticular activating system, leading to widespread vascular responses via local neurovascular coupling. Alternatively, spontaneous fluctuations could have their genesis in the cortex itself, perhaps taking the form of spatiotemporal waves upon the cortical sheet in a manner analogous to cortical slow waves (55). Finally, the neural and vascular responses could be modulated by a common input, either via parallel innervation or the release of factors that are both neuroactive and vasoactive. Whether such fluctuations serve to optimize the functionality of the cortex through periodic changes in excitability, to regulate the brain's metabolic load, or to reinforce existing functional connections, is presently a matter of speculation.

Determining the purpose and consequences of intrinsic events may prove to be of high importance for understanding the brain's most fundamental physiological principles. Converging data suggest that intrinsic activity, as opposed to sensory processing or motor execution, accounts for the majority of the brain's large energy consumption (56–58). It is intriguing to consider that synchronous global changes in neural activity, such as those pointed to in the present study, contribute significantly to this consumption.

Methods

Subjects and Testing. All procedures followed National Institutes of Health guidelines, were approved by the Animal Care and Use Committee, and were conducted with great care for the comfort and well-being of the animals. A total of 67 experimental runs (23, 27, and 17 runs in monkeys A, V, and S, respectively) were collected. Seven runs in monkey A, 19 runs in monkey V, and 4 runs in monkey S were excluded from further analysis, because the data did not show a consistent relationship between the neural and fMRI signals. Although this could reflect a genuine absence of physiological correlation in those sessions, post-hoc analysis revealed that the absence of any correlation was possibly due to (*i*) insufficient monocrystalline iron oxide nanoparticles (MION) concentration in the blood (in 8 excluded runs), (*ii*) poor LFP data quality, possibly caused by head movement artifacts (in 10 excluded runs), and (*iii*) an LFP-fMRI data synchronization problem (in 7 excluded runs); for the remaining 5 excluded runs the problem could not be determined. Apart from eye movements, no other physiological parameters were monitored.

Neurophysiological Recordings. Recordings of the local field potential from the implanted electrodes were conducted inside the scanner bore. Activity was recorded using an MR-compatible 32-channel amplifier with an input range of 16 mV (BrainAmp; Brain Products) and then passed optically out of the scanner bore. The amplifier was equipped with a 16-bit A/D converter, and sampled the signal at 5 kHz and a resolution of 500 nV. The signal was high-pass- and low-pass-filtered at 0.5 and 1,000 Hz, respectively. During simultaneous acquisition, the scanner was synchronized to the electrophysiological data via a brief digital pulse delivered at the beginning of each volume acquisition (BrainAmp; Brain Products).

MR Data Analysis. Functional (EPI) raw images were converted from the generic Bruker into the common Analysis of Functional NeuroImages (AFNI) data format. All images of a scan were realigned to correct for motion artifacts using a custom-written algorithm (Robert Cox, Scientific Statistical Computing Core, NIMH, Bethesda, MD). Functional data were registered to the corresponding high-resolution anatomical scan (Modified Driven Equilibrium Fourier Transform [MDEFT]) acquired before surgery using the analysis package mrVista (http://white.stanford.edu). Each voxel's time course was converted into units of percent change by first subtracting and then dividing by the mean of its time course.

Neuronal Data Analysis. Data were preprocessed using Vision Analyzer Software version 1.05 (Brain Products). Data were band-pass-filtered at 2–80 Hz, down-sampled to 200 Hz, and further analyzed in MATLAB (http://www.mathworks.com). Only segments of the LFP recorded during the 1-s gap between volume acquisitions were considered for analysis (i.e., none of the LFP signal obtained during 1.6-s periods of MR image acquisition was analyzed; *SI Text*). Segments containing clear movement artifacts were removed by an automated algorithm. Within each 1-s time window, the frequency-specific power was computed in two ways. First, using the FFT, the signal magnitude at all frequencies (2–100 Hz) was computed for each segment (i.e., for each repetition time; TR). For each frequency and time point, the magnitude estimates thus formed a family of time-varying signals at a sampling rate of the TR (albeit computed using the gap period only). This time-frequency LFP power matrix (i.e., spectrogram) served as the LFP signal representation that was then correlated with the rCBV (Fig. 2*A*), with the temporal cross-correlation of each frequency computed independently. Second, based on the zones of high and low correlation observed in this first approach, analysis then focused on three frequency ranges (Fig. 2*B*). The LFP signals were band-pass-filtered using a second-order Chebyshev filter into the following frequency bands: low (2–15 Hz), middle (15–40 Hz), and high (40–80 Hz), and then rectified. The mean over each segment was then computed. This analysis provided three estimates of time-varying band-limited power (BLP, or more precisely, the root-mean-square of the frequency-band-limited voltage).

Correlation of Neurophysiological and fMRI Signals. The time course of the neural signal measured from the electrode (either in the form of time-varying FFT magnitudes or BLP estimates) was evaluated for all voxels inside and outside the brain. Given that a certain neural event is likely to be associated with a hemodynamic event occurring later in time (owing to the nature of the hemodynamic response function), we computed the cross-correlation function between the fMRI and electrophysiological signal at lags up to $\pm$39 s (15 TRs). Initial analysis showed that the strongest correlation peaks (for the gamma range) were found at lags between 5.2 and 7.8 s. The value of this peak was taken as a measure of the correspondence between the electrophysiological and (inverted) CBV signal at voxels, and provided spatial maps of spontaneous activity. Unthresholded correlation coefficients were then rendered onto a 3D reconstruction of the anatomical scan for the three monkeys individually (mrVista). For the cross-correlation plots, mean voxel time courses were computed from a region of interest in each monkey. This ROI consisted of nine voxels in a sphere, corresponding to 30 mm^3 of gray matter cortex near the V1 electrode position. A control ROI was located in the white matter.

Information regarding the surgical procedures and MR scanning details is provided in *SI Methods*.

ACKNOWLEDGMENTS. We thank C. Zhu and K. Smith for assisting with the experiments, Dr. M. Schmid for help with the fMRI analysis, G. Dold, D. Ide, and T. Talbot for design and machining of MR-compatible materials used for data collection, and Drs. A. Silva, J. Walters, and A. Shmuel for discussion. Research was supported by the Intramural Programs of the National Institute of Mental Health, National Institute of Neurological Disorders and Stroke, and National Eye Institute. M.L.S. was supported by the Wellcome Trust.

1. Arieli A, Shoham D, Hildesheim R, Grinvald A (1995) Coherent spatiotemporal patterns of ongoing activity revealed by real-time optical imaging coupled with single-unit recording in the cat visual cortex. *J Neurophysiol* 73:2072–2093.
2. Arieli A, Sterkin A, Grinvald A, Aertsen A (1996) Dynamics of ongoing activity: Explanation of the large variability in evoked cortical responses. *Science* 273:1868–1871.
3. Leopold DA, Logothetis NK (2003) Spatial patterns of spontaneous local field activity in the monkey visual cortex. *Rev Neurosci* 14:195–205.
4. Leopold DA, Murayama Y, Logothetis NK (2003) Very slow activity fluctuations in monkey visual cortex: Implications for functional brain imaging. *Cereb Cortex* 13: 422–433.

5. Snodderly DM, Gur M (1995) Organization of striate cortex of alert, trained monkeys (*Macaca fascicularis*): Ongoing activity, stimulus selectivity, and widths of receptive field activating regions. *J Neurophysiol* 74:2100–2125.
6. Biswal B, Yetkin FZ, Haughton VM, Hyde JS (1995) Functional connectivity in the motor cortex of resting human brain using echo-planar MRI. *Magn Reson Med* 34: 537–541.
7. Vincent JL, et al. (2007) Intrinsic functional architecture in the anaesthetized monkey brain. *Nature* 447:83–86.
8. Fox MD, et al. (2005) The human brain is intrinsically organized into dynamic, anticorrelated functional networks. *Proc Natl Acad Sci USA* 102:9673–9678.
9. Friston KJ (1994) Functional and effective connectivity in neuroimaging: A synthesis. *Hum Brain Mapp* 2:56–78.
10. Greicius MD, Krasnow B, Reiss AL, Menon V (2003) Functional connectivity in the resting brain: A network analysis of the default mode hypothesis. *Proc Natl Acad Sci USA* 100:253–258.
11. Horwitz B (2003) The elusive concept of brain connectivity. *Neuroimage* 19:466–470.
12. Fox MD, Corbetta M, Snyder AZ, Vincent JL, Raichle ME (2006) Spontaneous neuronal activity distinguishes human dorsal and ventral attention systems. *Proc Natl Acad Sci USA* 103:10046–10051.
13. Rissman J, Gazzaley A, D'Esposito M (2004) Measuring functional connectivity during distinct stages of a cognitive task. *Neuroimage* 23:752–763.
14. Horovitz SG, et al. (2009) Decoupling of the brain's default mode network during deep sleep. *Proc Natl Acad Sci USA* 106:11376–11381.
15. Larson-Prior LJ, et al. (2009) Cortical network functional connectivity in the descent to sleep. *Proc Natl Acad Sci USA* 106:4489–4494.
16. Greicius MD, et al. (2008) Persistent default-mode network connectivity during light sedation. *Hum Brain Mapp* 29:839–847.
17. Martuzzi R, Ramani R, Qiu M, Rajeevan N, Constable RT (2010) Functional connectivity and alterations in baseline brain state in humans. *Neuroimage* 49:823–834.
18. Peltier SJ, et al. (2005) Functional connectivity changes with concentration of sevoflurane anesthesia. *Neuroreport* 16:285–288.
19. Pawela CP, et al. (2008) Resting-state functional connectivity of the rat brain. *Magn Reson Med* 59:1021–1029.
20. Majeed W, Magnuson M, Keilholz SD (2009) Spatiotemporal dynamics of low frequency fluctuations in BOLD fMRI of the rat. *J Magn Reson Imaging* 30:384–393.
21. van Eijsden P, Hyder F, Rothman DL, Shulman RG (2009) Neurophysiology of functional imaging. *Neuroimage* 45:1047–1054.
22. Moeller S, Nallasamy N, Tsao DY, Freiwald WA (2009) Functional connectivity of the macaque brain across stimulus and arousal states. *J Neurosci* 29:5897–5909.
23. Beckmann CF, DeLuca M, Devlin JT, Smith SM (2005) Investigations into resting-state connectivity using independent component analysis. *Philos Trans R Soc Lond B Biol Sci* 360:1001–1013.
24. Damoiseaux JS, et al. (2006) Consistent resting-state networks across healthy subjects. *Proc Natl Acad Sci USA* 103:13848–13853.
25. Fox MD, Raichle ME (2007) Spontaneous fluctuations in brain activity observed with functional magnetic resonance imaging. *Nat Rev Neurosci* 8:700–711.
26. Bianciardi M, et al. (2009) Modulation of spontaneous fMRI activity in human visual cortex by behavioral state. *Neuroimage* 45:160–168.
27. Eckert MA, et al. (2008) A cross-modal system linking primary auditory and visual cortices: Evidence from intrinsic fMRI connectivity analysis. *Hum Brain Mapp* 29: 848–857.
28. Cordes D, et al. (2000) Mapping functionally related regions of brain with functional connectivity MR imaging. *AJNR Am J Neuroradiol* 21:1636–1644.
29. Xiong J, Parsons LM, Gao JH, Fox PT (1999) Interregional connectivity to primary motor cortex revealed using MRI resting state images. *Hum Brain Mapp* 8:151–156.
30. Zhang D, et al. (2008) Intrinsic functional relations between human cerebral cortex and thalamus. *J Neurophysiol* 100:1740–1748.
31. O'Reilly JX, Beckmann CF, Tomassini V, Ramnani N, Johansen-Berg H (2010) Distinct and overlapping functional zones in the cerebellum defined by resting state functional connectivity. *Cereb Cortex* 20:953–965.
32. Di Martino A, et al. (2008) Functional connectivity of human striatum: A resting state fMRI study. *Cereb Cortex* 18:2735–2747.
33. Hagmann P, et al. (2008) Mapping the structural core of human cerebral cortex. *PLoS Biol* 6:e159.
34. Honey CJ, et al. (2009) Predicting human resting-state functional connectivity from structural connectivity. *Proc Natl Acad Sci USA* 106:2035–2040.
35. Bianciardi M, et al. (2009) Sources of functional magnetic resonance imaging signal fluctuations in the human brain at rest: A 7 T study. *Magn Reson Imaging* 27: 1019–1029.
36. Birn RM, Diamond JB, Smith MA, Bandettini PA (2006) Separating respiratory-variation-related fluctuations from neuronal-activity-related fluctuations in fMRI. *Neuroimage* 31:1536–1548.
37. Wise RG, Ide K, Poulin MJ, Tracey I (2004) Resting fluctuations in arterial carbon dioxide induce significant low frequency variations in BOLD signal. *Neuroimage* 21: 1652–1664.
38. Bianciardi M, van Gelderen P, Duyn JH, Fukunaga M, de Zwart JA (2009) Making the most of fMRI at 7 T by suppressing spontaneous signal fluctuations. *Neuroimage* 44: 448–454.
39. Murphy K, Birn RM, Handwerker DA, Jones TB, Bandettini PA (2009) The impact of global signal regression on resting state correlations: Are anti-correlated networks introduced? *Neuroimage* 44:893–905.
40. Fox MD, Zhang D, Snyder AZ, Raichle ME (2009) The global signal and observed anticorrelated resting state brain networks. *J Neurophysiol* 101:3270–3283.
41. Shmuel A, Leopold DA (2008) Neuronal correlates of spontaneous fluctuations in fMRI signals in monkey visual cortex: Implications for functional connectivity at rest. *Hum Brain Mapp* 29:751–761.
42. Nir Y, et al. (2008) Interhemispheric correlations of slow spontaneous neuronal fluctuations revealed in human sensory cortex. *Nat Neurosci* 11:1100–1108.
43. He BJ, Snyder AZ, Zempel JM, Smyth MD, Raichle ME (2008) Electrophysiological correlates of the brain's intrinsic large-scale functional architecture. *Proc Natl Acad Sci USA* 105:16039–16044.
44. Logothetis NK, Pauls J, Augath M, Trinath T, Oeltermann A (2001) Neurophysiological investigation of the basis of the fMRI signal. *Nature* 412:150–157.
45. Shmuel A, Augath M, Oeltermann A, Logothetis NK (2006) Negative functional MRI response correlates with decreases in neuronal activity in monkey visual area V1. *Nat Neurosci* 9:569–577.
46. Niessing J, et al. (2005) Hemodynamic signals correlate tightly with synchronized gamma oscillations. *Science* 309:948–951.
47. Belitski A, et al. (2008) Low-frequency local field potentials and spikes in primary visual cortex convey independent visual information. *J Neurosci* 28:5696–5709.
48. Macey PM, Macey KE, Kumar R, Harper RM (2004) A method for removal of global effects from fMRI time series. *Neuroimage* 22:360–366.
49. Logothetis NK (2002) The neural basis of the blood-oxygen-level-dependent functional magnetic resonance imaging signal. *Philos Trans R Soc Lond B Biol Sci* 357: 1003–1037.
50. Attwell D, Iadecola C (2002) The neural basis of functional brain imaging signals. *Trends Neurosci* 25:621–625.
51. Viswanathan A, Freeman RD (2007) Neurometabolic coupling in cerebral cortex reflects synaptic more than spiking activity. *Nat Neurosci* 10:1308–1312.
52. Sirotin YB, Das A (2009) Anticipatory haemodynamic signals in sensory cortex not predicted by local neuronal activity. *Nature* 457:475–479.
53. Maier A, et al. (2008) Divergence of fMRI and neural signals in V1 during perceptual suppression in the awake monkey. *Nat Neurosci* 11:1193–1200.
54. Nir Y, et al. (2007) Coupling between neuronal firing rate, gamma LFP, and BOLD fMRI is related to interneuronal correlations. *Curr Biol* 17:1275–1285.
55. Massimini M, Huber R, Ferrarelli F, Hill S, Tononi G (2004) The sleep slow oscillation as a traveling wave. *J Neurosci* 24:6862–6870.
56. Raichle ME, Mintun MA (2006) Brain work and brain imaging. *Annu Rev Neurosci* 29: 449–476.
57. Attwell D, Laughlin SB (2001) An energy budget for signaling in the grey matter of the brain. *J Cereb Blood Flow Metab* 21:1133–1145.
58. Shulman RG, Rothman DL, Behar KL, Hyder F (2004) Energetic basis of brain activity: Implications for neuroimaging. *Trends Neurosci* 27:489–495.